CHAPTER 6

Ever increasing concern regarding energy saving and environment protection has driven an interest towards development of energy-efficient lubricant additives which may possess superior tribological properties but lower emissions than those of the conventionally used additives. As discussed in the previous chapter, addition of nanomaterials as additives in base lubricant oil is a rapidly progressing field of research because nanomaterials are different from traditional bulk materials due to their extremely small size and high specific surface area [Liang *et al*.(2013)].

Graphene has drawn attention due to its exceptional electrical [Berman *et al*.(2014), Vicarelli *et al*.(2015)], optical [Corato *et al*.(2014)], thermal [Zhu *et al*.(2013)] and mechanical properties [Berman *et al*.(2014), Zhu *et al*.(2013)]. In recent years, graphene based materials have been extensively studied for their potential applications in electronic [Ritter *et al*.(2009)], sensor and catalytic properties [Yasaei *et al*.(2014), Benson *et al*.(2014)]. Graphene has been recognized as an excellent candidate for reducing adhesion, friction and wear, however, its application in lubrication field has not been explored significantly [Meng *et al*.(2015), Mungse *et al*.(2014)]. Graphene being two-dimensional material, offers unique friction and wear properties which are not typically seen in conventional materials. It has been demonstrated to act as an effective solid lubricant and/or lubricating oil additive [Meng *et al*.(2015)]. High chemical inertness, extreme strength, and easy shear ability on its densely packed and atomically smooth surface are the major favourable attributes for its remarkable tribological behavior. From a tribological point of view, such extreme mechanical strength is highly desirable for wear protection. Graphene has been shown to be impermeable to liquids and gases, such as water or oxygen, thus slowing down the corrosive and oxidative processes that usually cause more damage to the rubbing surfaces [Berman *et al*.(2014)]. The number of layers, degree of defects and preparation methods etc. play an important role towards its friction, wear and adhesion properties [Mungse *et al*.(2014)]. The properties like high specific surface area, low shear strength, excellent Young's modulus, high thermal stability, good conductivity etc., are desirable in a material from lubrication point of view. A literature survey reveals that graphene possesses all of these desirable properties [Mungse *et al.(*2014)].

Kim *et al.*(2011) have investigated the micro-scale tribological behavior of multilayer graphene using atomic force microscopy technique and found lower friction values but graphene detached when sliding was performed under an applied load of 5μN for 100 cycles. Berman *et al.*(2014) have studied the macro-scale tribological properties of graphene dispersed in ethanol. The results indicate that graphene reduced the friction coefficient greatly but was instantly removed from the sliding surface under an applied load of 5N. Therefore, an intermittent supply of graphene was needed to ensure its presence throughout the whole test period.

One possible approach to improve the tribological properties of graphene and utilize the above mentioned advantages for tribological applications would be with the hybrid-graphene based materials which can implement the synergistic enhancement effect. In the field of tribology, boron and nitrogen based additives have received much attention showing synergistic behavior via formation of *in situ* protective boron nitride tribochemical film between the steel-steel interface, thereby minimizing friction and wear [Jaiswal *et al.*(2014a)]. During past several decades, some 3d-transition metal compounds have been used as reinforcing materials [How *et al.*(2014), Jia *et al.*(2015), Guo *et al.*(2015)].Among the 3d-transition elements, titanium dioxide (TiO_2) nanoparticles seem to be fascinating for remarkable tribological behavior [Sabareesh *et al.*(2012)]. Therefore, in order to drastically reduce friction and wear simultaneously under a high load, the TiO_2-reinforced boron, nitrogen-co-doped-microwave assisted reduced graphene oxide (TiO_2-B-N-MRG) hybrids have been synthesized.

Herein, in the present chapter, we have synthesized MRG, boron doped-MRG (B-MRG), nitrogen doped-MRG (N-MRG), boron, nitrogen co-doped-MRG (B-N-MRG) and titanium dioxide reinforced-boron, nitrogen co-doped-MRG (TiO_2-B-N-MRG) hybrid materials and characterized them by various state-of-the-art techniques. The resulting graphene based hybrid materials are employed as lubricating additives in neutral paraffin oil and their tribological properties are systematically studied using four-ball lubricant testing machine. The obtained results show that the addition of small amount of MRG in base lube significantly enhanced the tribological properties of base lube. Besides this, doping of hetero-atoms nitrogen, boron and co-doped boron and nitrogen to MRG successively enhanced the antiwear properties of the

MRG by virtue of forming a protective *in situ* tribochemical film at the steel-steel interface. Furthermore, the load bearing characteristics of B-N-co-doped-MRG are remarkably improved upon reinforcement with TiO_2 nanoparticles. The surface characterization of the interacting tribopairs has been done with the help of Scanning Electron Microscopy (SEM) and contact mode Atomic Force Microscopy (AFM).

6.1. Experimental section

6.1.1. Materials

All materials used in the synthesis were of Analytical Reagent grade and employed without any further purification. These include titanium (IV) butoxide, ($C_{16}H_{36}O_4Ti$, Sigma-Aldrich, purity >97%), graphite flakes (1-2 mm, NGS Naturgraphit GmbH), potassium permanganate ($KMnO_4$, ≥99.0%, Fluka), ethanol (CH_3CH_2OH, ≥98% Sigma-Aldrich) and boric acid (H_3BO_3, ≥98% Sigma-Aldrich). The other chemicals such as ammonia solution, H_2SO_4, H_3PO_4, H_2O_2, $N_2H_4.H_2O$, etc. were procured from Merck, India.

6.1.2. Synthesis of graphene based nanomaterials

6.1.2.1. Preparation of Graphene Oxide and Reduced Graphene Oxide

Graphene oxide (GO) have been synthesized using chemical route as suggested by Marcano *et al*.(2010) with some modifications, as briefly described here. Initially, 2g of graphite flakes were added to concentrated H_2SO_4/H_3PO_4 (9:1) solution and stirred on a magnetic stirrer followed by slow addition of 6 weight equivalent of $KMnO_4$ (12g). Addition of $KMnO_4$ was done very slowly to avoid any kind of explosion. The mixture was stirred for 12h at a constant temperature of 50 °C. Afterwards, the mixture was cooled to room temperature and the reaction was quenched by adding ca. 270mL of ice with slow addition of 2mL H_2O_2 (30%) as the reaction is highly exothermic. The mixture was then filtered, shifted, and centrifuged. The obtained solid material was washed with distilled water, 30% HCl and ethanol until the pH≈7 was reached. The material was then dried at 80 °C. Finally, the exfoliated graphene oxide dispersion was obtained for further experiments. The conversion of GO to reduced graphene oxide (MRG) was achieved using microwave-assisted thermal expansion method by microwave irradiation of 700 W for 40s.

6.1.2.2. Preparation of TiO_2 Nanoparticles

TiO_2 nanoparticles were synthesized by a sol-gel method with slight modification [Kozlova *et al*.(2012)]. Concentrated HNO_3 (3mL), absolute ethanol (35 mL) and de-ionized water (15mL) were mixed together and to the resulting mixture 17mL of titanium butoxide (50mmol) dissolved in 40mL of absolute ethanol was added drop-wise. It was stirred for 90 min. After 30h the product light white TiO_2 gel was filtered and dried at 200°C for 6h. The pale yellow nanoparticles obtained were used for other characterizations and further synthesis of TiO_2-reinfonced B-N-co-doped reduced graphene oxide.

6.1.2.3. Preparation of doped-Reduced Graphene Oxide

Boron-doped reduced graphene oxide (B-MRG), nitrogen-doped reduced graphene oxide (N-MRG) and Boron-Nitrogen co-doped reduced graphene oxide (B-N-MRG) have been synthesized by microwave assisted method. For the preparation of B-MRG, 500mg of GO was dispersed in ethanol (50ml) in bath sonicator followed by ultra sonicator to make uniform suspension. Boric acid solution (1mg/mL) was added to GO solution under stirring condition and kept at 60°C for 8h. After completion of the reaction, mixture was cooled to room temperature and washed with deionised water. The obtained black powder was dried at 80°C and kept in microwave oven for 3 min at 700W. The final black powder of B-MRG is very light in weight. Similarly, N-MRG has been synthesized using ammonia solution in place of boric acid. Further, Boron-Nitrogen co-doped reduced graphene oxide (B-N-MRG) has been synthesized by adding ammonia and boric acid solution simultaneously under vigorous stirring and following the above procedure, Scheme 6.1.

6.1.2.4. Preparation of TiO_2-B-N-co-doped Reduced Graphene Oxide

For the preparation of TiO_2 nanoparticles dispersion, 900mg of TiO_2 nanoparticles were well dispersed in 100mL of ethanol (96%) by sonicating it for an hour at ~50°C. B-N-doped MRG suspension (1mg/mL) in ethanol (96%) was made similarly. The hybrid material was prepared by mixing the both suspensions under stirring condition. The mixture was sonicated for an hour at ~70°C. The hybrid material was filtered and dried at 45°C. The black powder was kept in a microwave oven for 3 min at 700W and cotton like black product (TiO_2-B-N-MRG) was obtained.

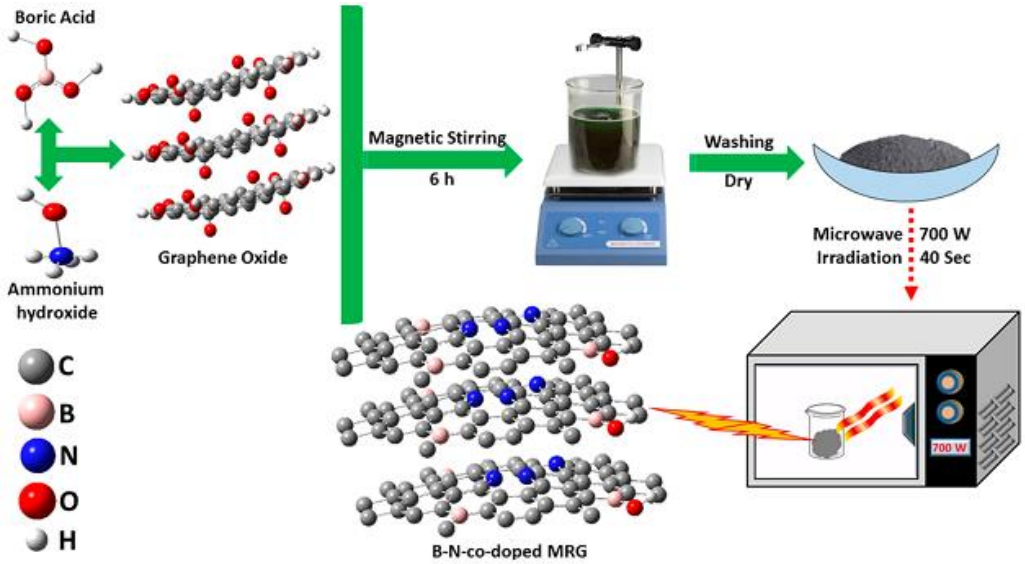

Scheme 6.1. Microwave assisted approach for the preparation of B-N-co-doped-MRG nanomaterials

6.1.3. Dispersion stability

To evaluate the dispersion stability of as prepared various MRGs nanomaterials in liquid paraffin oil, the individual nanomaterial was ultrasonically dispersed in paraffin for 1h. The concentration of these additives in paraffin oil was optimized as 0.15% w/v according to the results of tribological tests and these solutions were further diluted 10 times in order to record their UV-Vis spectra. Dispersion stability of the MRGs in base oil was examined by means of absorbance measurement at different time intervals. The photographs of the neutral paraffin oil containing different additives were taken and different settling times were observed.

6.1.4. Tribological Characterization

Paraffin oil blends of various synthesized graphene based materials having concentrations 0.00, 0.05, 0.10, 0.15 and 0.20 % (w/v) were made by stirring at 40-50 $^{\circ}$C for 2h and thereafter sonicating for 1h at room temperature. The entire tribological tests were carried out at an optimized concentration i.e., 0.15% w/v of MRG, B-MRG, N-MRG, B-N-MRG and TiO_2-B-N-MRG in paraffin as a base lube.

6.2. Results and discussion

6.2.1. Morphology and Microstructure of MRGs

The SEM images of MRG, B-N-MRG and TiO_2-B-N-MRG are presented in Figure 6.1. Layered structure of graphene is conspicuous from the SEM images of

MRG, Figure 6.1a. After co-doping of B and N to MRG (Figure 6.1b) the morphology appears to be almost unchanged. In Figure 6.1c, it is clearly visible that TiO_2 nanoparticles (2-15 nm) are decorated on graphene sheet. Further, to confirm the chemical composition of TiO_2-B-N-MRG, energy dispersive X-ray spectra (EDX) of as synthesized samples were recorded. EDX spectrum of TiO_2-B-N-MRG (Figure 6.1c) clearly shows strong signal for carbon but the signals for B and N separately could not be identified owing to their small amount as dopant and close atomic number with C. The quantitative EDX results, tabulated in inset of Figure 6.1c reveal an approximate stoichiometric composition as TiO_2-B-N-MRG. The signals from oxygen (~10.27% atomic weight) and titanium (~14.79% atomic weight) confirmed the presence of TiO_2 nanoparticle on the graphene sheet.

The morphology of all samples was further characterized by TEM and HRTEM also. TEM images of MRG, B-N-MRG and TiO_2-B-N-MRG (Figures 6.2a, c and e) show transparent and layered structure. After co-doping of B and N, slight changes are observed in graphene morphology. The HRTEM images (Figures 6.2b and d) show the lattice spacing of graphene sheets in MRG and B-N-MRG as 0.339 and 0.34nm respectively due to 002 plane of graphene. Figures 6.2e and 2f display the TEM and HRTEM images of TiO_2-B-N-MRG exhibiting clearly TiO_2 nanoparticles on the surface of doped graphene. The size of TiO_2 nanoparticles is found to be in the range of 2-15 nm with several crystal planes which are randomly oriented across the particles. The high-resolution TEM image of the TiO_2-B-N-MRG exhibits the lattice fringes of the TiO_2 (0.352 nm) corresponding to the TiO_2 (101) plane (JCPDS No. 21-1272) and lattice spacing of graphene sheets was found to be 0.343nm corresponding to 002 plane of graphene.

Typical X-ray diffraction (XRD) patterns of MRG, B-MRG, N-MRG, B-N-MRG and TiO_2-B-N-MRG are shown in Figure 6.3a. In the diffraction pattern of MRG, the peak around 26.13° corresponds to the (002) reflection (interlayer spacing of 0.35 nm) while the other peak at 43.7° having lower intensity compared to the previous peak corresponds to the (100) reflection implying the formation of turbostratic graphitic carbon [Li et al.(2007)]. The XRD pattern of TiO_2 nanoparticles reported six distinct diffraction peaks at 20.8°, 25.1°, 30.4°, 37.9°, 48.2°, and 54.2° indexed with the (102), (101), (101), (004), (200) and (105) planes of TiO_2 (JCPDS no. 21-1272) respectively, in a fcc crystal structure. The presence of distinct broad peaks confirms the high purity of the prepared nanoparticles with small size. The interplanar spacing of d_{002} plane, crystallite size and lattice parameters of MRG, B-

MRG, N-MRG and B-N-MRG samples, calculated using Bragg's law and Debye-Scherrer's formula show non-remarkable variations. Furthermore, it can be found that the XRD patterns of TiO_2-B-N-MRG show peaks which are similar to the diffraction pattern of TiO_2. This indicates that the anatase phase is predominant in the composite sample. The XRD pattern of TiO_2-B-N-MRG exhibits clear peaks of pure TiO_2, but the peak at 25° in TiO_2 is broadened due to its superimposition with the diffraction peak of MRG at 24.04°. The highlighted diffraction peak in Figure 6.3a (~25°) deconvoluted into three diffraction peaks corresponding to anatase, rutile phase and graphitic. Figure 6.3b shows deconvoluted peaks corresponding to (101) (003) and (002) reflection planes.

Additional structural information of the MRG, N-MRG, B-MRG, B-N-MRG and TiO_2-B-N-MRG nanomaterials was availed from Raman spectroscopy using 532 nm laser excitations are shown in Figure 6.4a. The D peak at approx. 1359 cm^{-1} is due to a breathing mode of A1g symmetry, which is endorsed to the presence of disorder in graphene sheets. The G peak at ca. 1586 cm^{-1} is a doubly degenerate phonon mode (E2g symmetry) for sp^2 carbon network which is showcase of graphitic nature of compound [Ferrari *et al.*(2000)]. The 2D band in Raman spectra of graphene is overtone of D band and it is susceptible to the stacking order of graphene layers resulting in turbostratic graphite, which lacks a stacking order of graphene layers. Presence of this band shows turbostratic graphite. In graphene with multilayers, 2D band is ascribed to the presence of 2-D and 3-D graphite structure [Barros *et al.*(2005)]. Since 2D band originates from a process where two phonons with opposite wave-vectors satisfy momentum conservation, therefore no defects are required for the activation of 2D bands and this peak is always present in all samples. The ratio of intensity of D and G band (I_D/I_G ratio), demonstrates the density defects and hence the degree of disorder in the structure. The I_D/I_G ratio is found to increase from 0.4159 in graphene to 0.5506 and 0.5852 after doping of B and N respectively. This confirms that disorder has appreciably increased in graphene sheet [Reddy *et al.*(2010)]. However, after co-doping of B and N and decoration of TiO_2 nanoparticle, the I_D/I_G ratio is decreased from 0.4159 to 0.2625 and 0.1629 which may be due to rearrangement of sp^2 carbon and more reduction of oxygen. Raman spectrum of TiO_2 nanoparticles shows five Raman peaks, Figure 6.4b. The peaks observed around 148, 267, 402, 514 and 638 cm^{-1} are assigned to the E(g), E(g), B(1g), B(1g)+ A(1g), and the E(g) modes of anatase phase respectively.

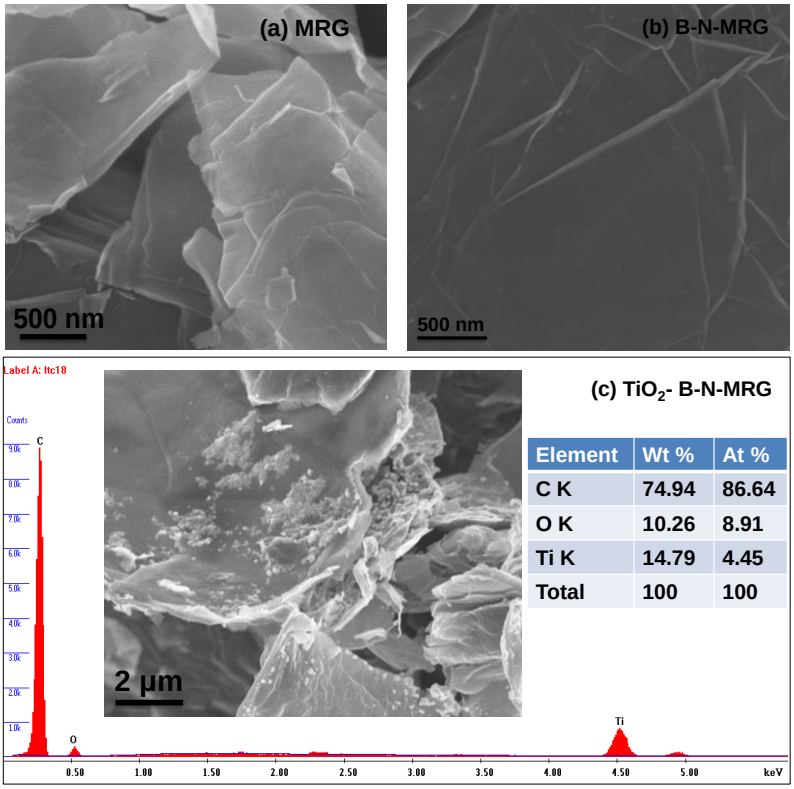

Figure 6.1. SEM images of (a) MRG, (b) B-N-MRG and (c) TiO_2-B-N-MRG with EDX spectrum

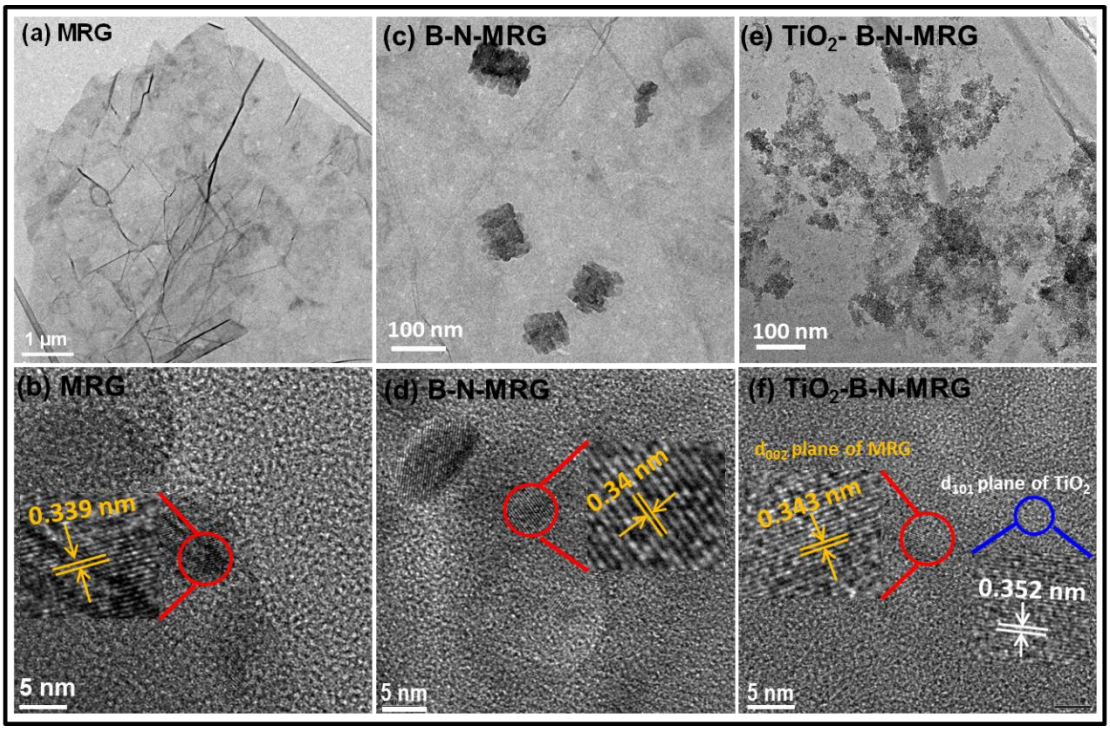

Figure 6.2. TEM and HRTEM images respectively for MRG (a and b), B-N-MRG (c and d) and TiO_2-B-N-MRG (e and f)

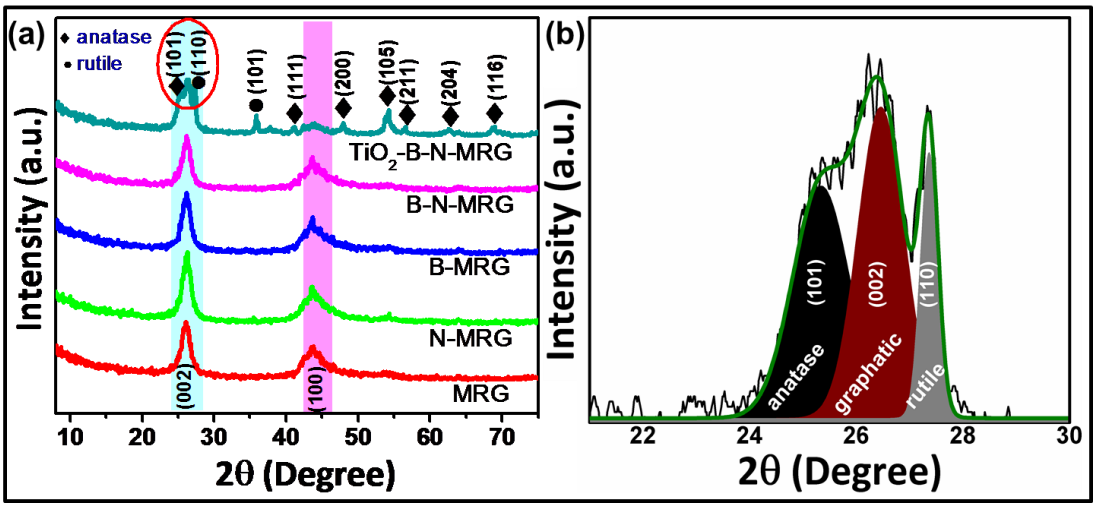

Figure 6.3. XRD diffraction pattern of MRGs nanomaterials (a) and the highlighted peak with red circle fitted with three different peak (b)

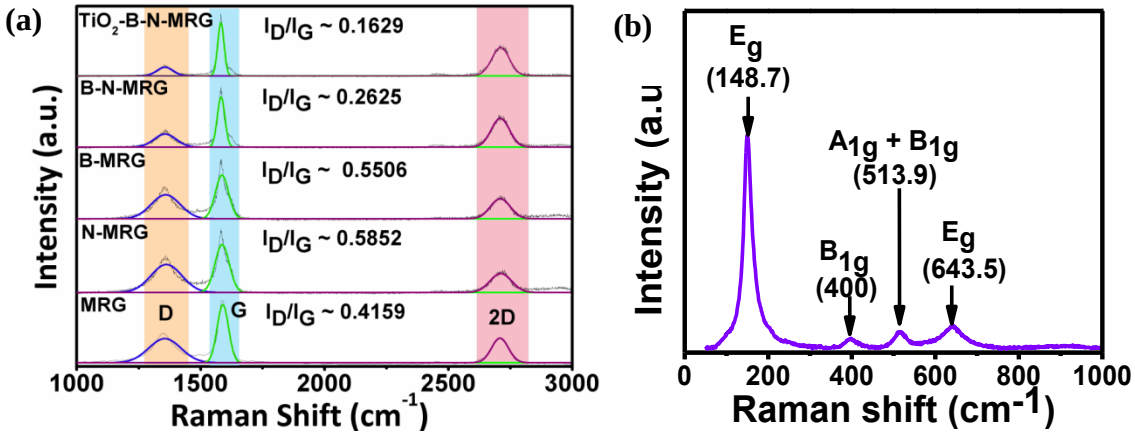

Figure 6.4. Raman spectra of (a). MRGs samples and (b). TiO_2 nanoparticles

Further, the chemical structures of MRG and TiO_2-B-N-MRG were studied using XPS measurements. XPS survey of both MRG and TiO_2-B-N-MRG (**Figure 6.5a**) shows the presence of B, N and Ti elements with carbon and oxygen. Atomic % of C, O, B, N and Ti is 87.18, 8.07, 1.56, 2.42 and 0.77 respectively. Moreover, the core-level spectra of TiO_2-B-N-MRG have been deconvoluted with best fitting parameters using peak fit software as shown in **Figure 6.5**. **Figure 6.5b** shows that the core level spectra of C1s have been deconvoluted into six peaks with binding energies of 283.9, 284.7, 285.1, 286.3, 288.2 and 290.6 eV corresponding to B-C, sp^2C–sp^2C, N-sp^2C, N-sp^3C, C=O, and O-C=O bonds respectively [Han *et al.*(2013)]. B1s core level spectra can be deconvoluted into three components showing peaks at 191.5, 192.3 and 193.2 corresponding to B-C, B-CO_2 and B–O bonds respectively as shown in **Figure 6.5c** [Bourlinos *et al.*(2015)]. **Figure 6.5d** shows that N1s core level spectrum deconvoluted into three peaks corresponding to pyridinic N (~ 398.5 eV),

pyrrolic N (~ 399.5 eV) and graphitic N (398.5eV). Ti 2p core-level spectrum shows the presence of Ti $2p_{3/2}$ and Ti $2p_{1/2}$ levels, **Figure 6.5e** [Reddy *et al*.(2010)].

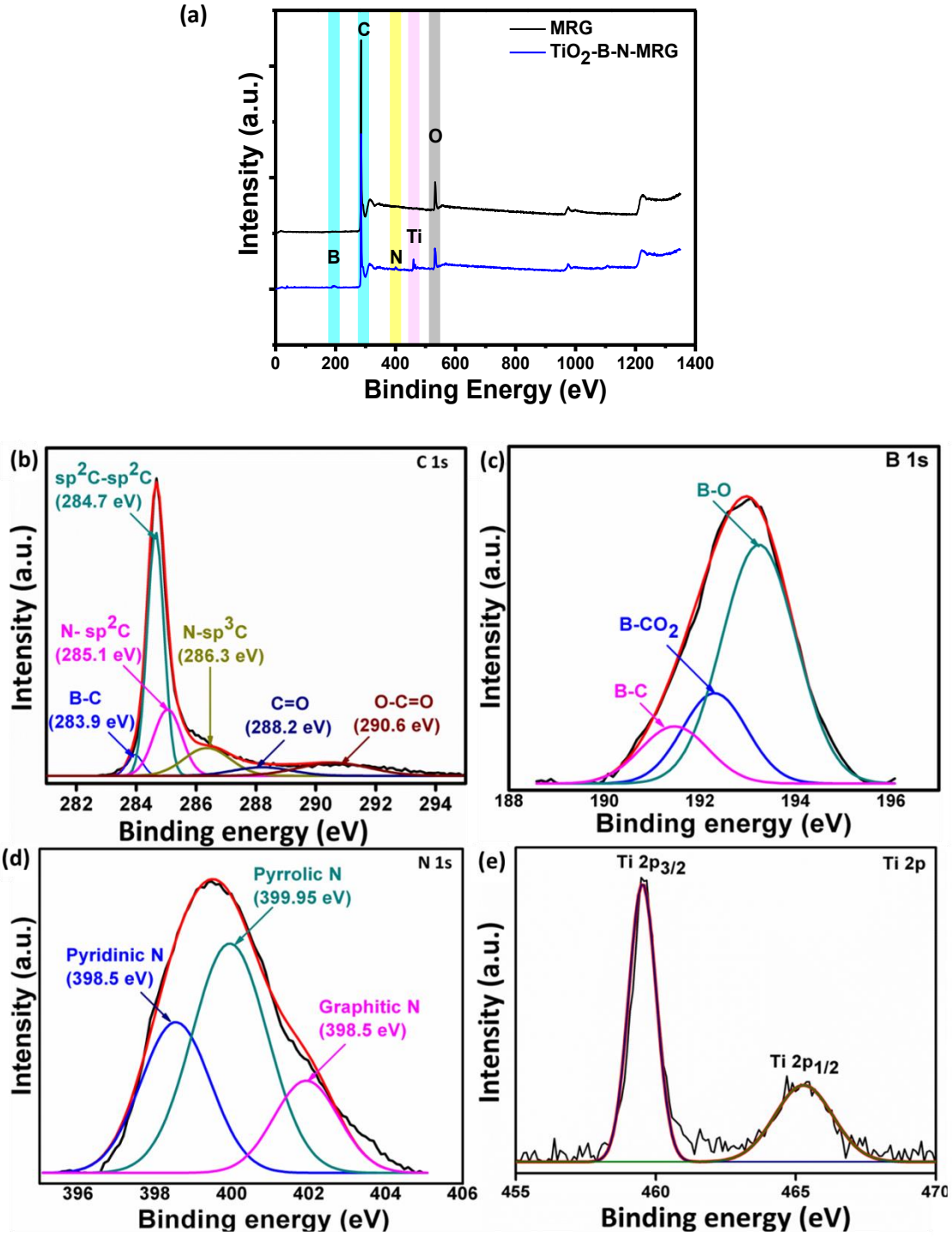

Figure 6.5. XPS survey spectra of (a) MRG and TiO_2-B-N-MRG samples and deconvoluted XPS spectra of TiO_2-B-N-MRG nanomaterial: (b) C1s core shell spectra, (c) B1s core shell spectra, (d) N1s core shell spectra and (e) Ti2p core shell spectra

6.2.2. Dispersion stability of MRGs in paraffin oil

The dispersion stability of MRG, B-MRG, N-MRG, B-N-MRG and TiO_2-B-N-MRG nanomaterials in paraffin oil was evaluated and compared using UV-visible spectroscopy. Figure 6.6a shows the relative absorbance of ultrasonically dispersed different samples in base oil w.r.t. time. The relative absorbance of MRGs in base oil reduces with time before getting settled down. The sedimentation of the MRG is comparatively much faster than the doped MRGs. With the expense of time, the relative absorbance of each nanomaterial decreases. Initially, upto 12h there is a marginal change (upto 10%) in the suspension stability of TiO_2-B-N-MRG and B-N-MRG whereas this change becomes significant (upto 18-25%) in case of B-MRG, N-MRG and MRG. However, after a long period of time exposure (48h), the relative absorbance of the B-N-MRG, TiO_2-B-N-MRG is maintained respectively at ~0.69 and ~0.70 which is much higher than the relative absorbance of MRG, B-MRG and N-MRG respectively ~0.48, ~0.59 and ~0.59. Thus, the dispersion stability of B-N-MRG and TiO_2-B-N-MRG is comparatively much higher than the pure MRG, B-MRG/N-MRG. Figure 6.6b shows optical images of different samples dispersed in paraffin oil at different periods. Initially, after sonication the different MRGs samples are well-dispersed in the base oil. After 48h of time exposure, the lubricants containing MRG, B-MRG and N-MRG appear to be almost settled down. On the other hand B-N-MRG and TiO_2-B-N-MRG remain suspended in the base lube up to 48h showing their maximum dispersion stability. Thus, the sedimentation plots and images of various MRG samples proved that the dispersion stability of graphene in paraffin oil can be improved upon co-doping with B and N and further reinforcement with TiO_2 nanoparticles.

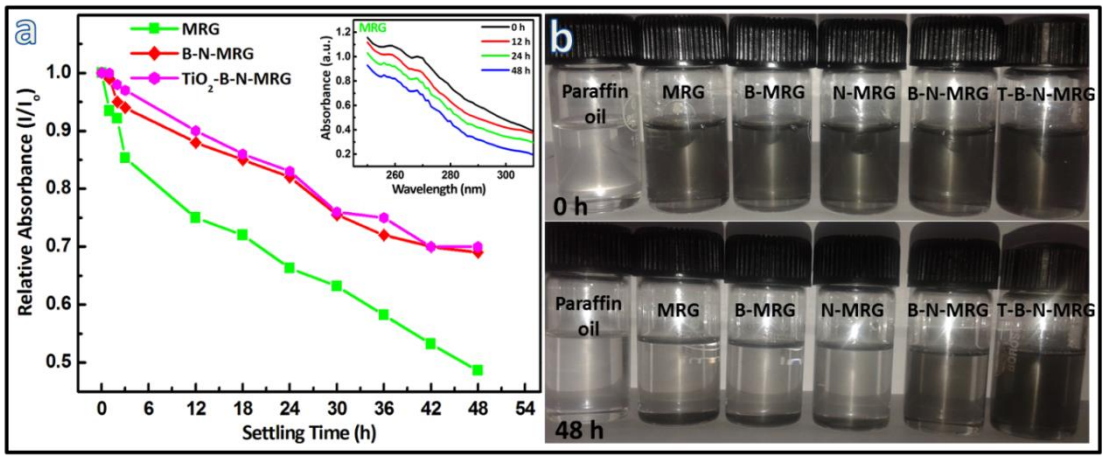

Figure 6.6. Dispersion stabilities of the pure oil containing MRG, B-N-MRG and TiO_2-B-N-MRG studied by UV-vis spectrophotometry (a), Optical photographs of the different MRGs samples dispersed in pure oil at different settling times (b)

6.2.3. Tribological Properties

6.2.3.1. Additive optimization

Antiwear behavior of the additive depends on its concentration in the base lube. Therefore, it is important to optimize the additive concentration before conducting the tribological test. Figure 6.7 shows the variation of mean wear scar diameter (MWD) with additive concentration at a load of 392N for 60 min test duration in paraffin as a base lube. Figure 6.7 shows that the blends of MRG and B-N-MRG in paraffin oil significantly reduced the MWD values and thereby improved the antiwear properties of base oil at each concentration. The MWD value decreases from 0.733 mm to 0.702 mm (in case of MRG) and 0.699 mm (in case of B-N-MRG) at the additive concentration of only 0.05% w/v. The antiwear performance of blends is further improved upon increasing their concentration to 0.10%. At this concentration, the advantage of B-N-co-doping in MRG over MRG can be clearly seen. It may be associated with the layered structure of MRG having boron and nitrogen atoms which have low shear strength and prevent metal-metal adhesion. Under operating conditions, these hetero atoms may interact with each-other and/or with the steel surface to form *in situ* protective films [Yan *et al*.(2014a,b)]. On further increasing the concentration up to 0.15%, the lowest values of MWD are obtained in case of both MRG (0.655mm) and B-N-MRG (0.490mm). However, on increasing the concentration from 0.15-0.20%, the MWD values began to slightly increase in each case which may be due to corrosive wear. Thus, the optimized additive concentration has been found to be 0.15% w/v and hence, all the tribological tests were performed at this optimized concentration.

6.2.3.2. Antiwear Properties

The synthesized graphene based hybrid materials were evaluated to probe their lubrication potential using paraffin as a base lube. The comparison of the mean wear scar diameter (MWD) along with average coefficient of friction (COF) values of the corresponding steel balls lubricated with base oil and blends of B-MRG, N-MRG, B-N-MRG, TiO_2-B-N-MRG hybrid materials in paraffin oil under the load of 392N for

60 min test duration at 1200 rpm (ASTM D4172) are shown in Figure 6.8. The value of MWD and average COF for paraffin oil were about 0.733mm and 0.0756, respectively. Addition of all nanomaterials as additive to the base lube significantly reduces the both MWD and COF. There is slight improvement in the antiwear properties of the base oil in presence of MRG which reduces the value of MWD and COF by only 10.64 and 02.91%, respectively. The extent of improvement in these values is increased upon doping of individual boron and nitrogen atoms to MRG. However, in case of boron-nitrogen-co-doped MRG these values increase further to a greater degree. The obtained results suggest that the blend of B-N-MRG has better lubricating behavior than the individual B-MRG and N-MRG which may be due to synergistic lubricating action of the boron and nitrogen atoms present in B-N-MRG. Under tribostress conditions, these atoms react with each other and/or with the interacting steel surface to form protective *in situ* tribochemical film/s which may be composed of boron nitride, B_2O_3 etc. The tribofilm separates the metal-metal contact at interface thereby reducing friction and wear [Jaiswal *et al*.(2014a)]. Low shear strength and high thermal conductivity of these protective tribofilms are beneficial for the excellent tribological properties [Wan *et al*.(2015)]. The lubricant also acts a as heat transfer medium which reduces the asperity temperature at steel-steel interface and prevents the surface from adhesion. Furthermore, the effect of reinforcement of B-N-MRG with TiO_2 nanoparticles is clearly evident from Figure 6.8 as it exhibits phenomenal reduction in the MWD and COF values about 50.88 and 25.40%, respectively which is much larger than those obtained in case of B-N-MRG (33.15 & 20.37%). The exceptional tribological behavior of TiO_2-B-N-MRG hybrid nanomaterial in paraffin oil is the cumulative effect of layered structure of MRG, synergistic interaction of boron and nitrogen; and the most important is the TiO_2 nanoparticles which act as nanobearings between steel-steel interfaces. Addition of even a very small concentration of graphene based hybrid materials to the base lube is sufficient for the formation of protective tribofilms on steel surfaces.

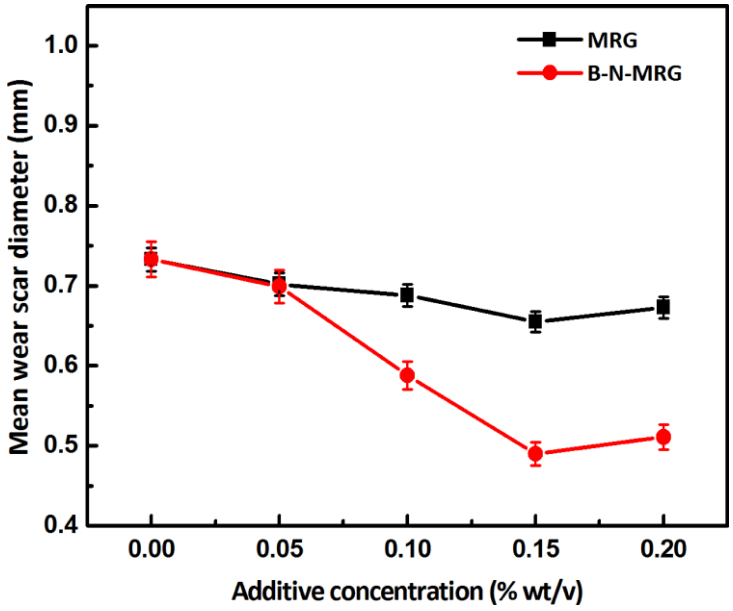

Figure 6.7. Variation of mean wear scar diameter for the paraffin oil as a function of increasing additive concentrations at 392N applied load and 60 min duration

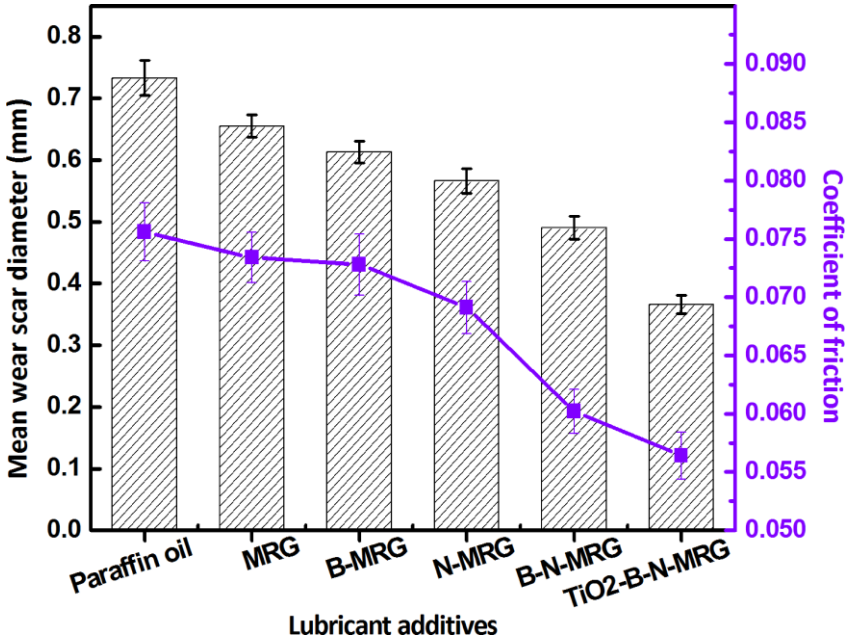

Figure 6.8. Variation in mean wear scar diameter and coefficient of friction in the presence of MRGs nanomaterials in paraffin oil. Load: 392N, sliding speed: 1200 rpm, temperature: 75 °C, test duration: 60 min., concentration of MRGs: 0.15 % w/v

Figure 6.9 illustrates the variation in the friction coefficient of steel surface supplemented with paraffin oil and blends of various graphene based hybrid nanomaterials in paraffin oil with time. One can see that the friction coefficient value

of the base oil varies considerably during the entire test duration and its values are higher and unstable than those for the base oil with additives. There is significant reduction in the COF for the blends of graphene based nanomaterials except MRG. The exceptional increase in the COF values of MRG with time may be due to the consequences of agglomeration of MRG under high temperature and pressure which hampered their uninterrupted supply to the interfaces. On the other hand, the friction coefficient of the base oil containing N-MRG, B-N-MRG and TiO_2-B-N-MRG remarkably decreases with time. This test confirms the formation of the tribofilm formed by these additives even at such a low concentration. In presence of additives, high COF values are obtained during initial few minutes of the sliding time and later on in all cases it gradually decreases and/or remains constant except MRG. The lowest and almost stable friction coefficient values are obtained for the surface lubricated with TiO_2-B-N-MRG which may be due to the presence of TiO_2 nanobearings at tribocontact thereby reducing friction. The initially obtained high friction values may be attributed to the absence of any tribofilm between steel-steel interfaces because formation of tribofilm is time dependent. The stability of the friction coefficient with time is a very important property in mechanical systems needed for their functionality during the service life [Shah *et al*.(2009)].

In order to investigate wear rate of the steel-steel surface supplemented with graphene based hybrid nanomaterials in paraffin oil the test has been also performed for different 15, 30, 45, 60, 75 and 90 time durations under the load of 392N at 0.15% w/v concentration. The obtained MWD values as a function of sliding time for different additives has been plotted in Figure 6.10. To estimate wear more accurately it is important to investigate the variation of mean wear volume with respect to time instead of mean wear scar diameter. Figure 6.11 shows the variation of mean wear volume with different sliding time and the linear regression model is fitted to obtained wear rate. The value of running-in and steady-state wear rate has been mentioned in Table 6.1. The values of running-in and steady-state wear rates are found to be very high in absence of additives; however, in presence of MRG, B-MRG, N-MRG, B-N-MRG and TiO_2-B-N-MRG hybrid nanomaterials these values are successively reduced in each case. Besides this, the values of running-in wear rate in each case are found to be larger than those of corresponding steady-state wear rate. The observed behavior of wear rates in presence of additives follows the same trend as discussed above. The lowest values of running-in and steady-state wear rates are found for the

surface added with TiO_2-B-N-MRG hybrid nanomaterials which reduce these values upto 24 and 67 folds, respectively in comparison to base lube. The life of engineering components is assessed on the basis of steady-state wear rate. Thus, on the basis of such a tremendously low steady-state wear rate, one can recommend these TiO_2-B-N-MRG hybrid nanomaterials for potential application in the tribological industries for wide range of lubrication.

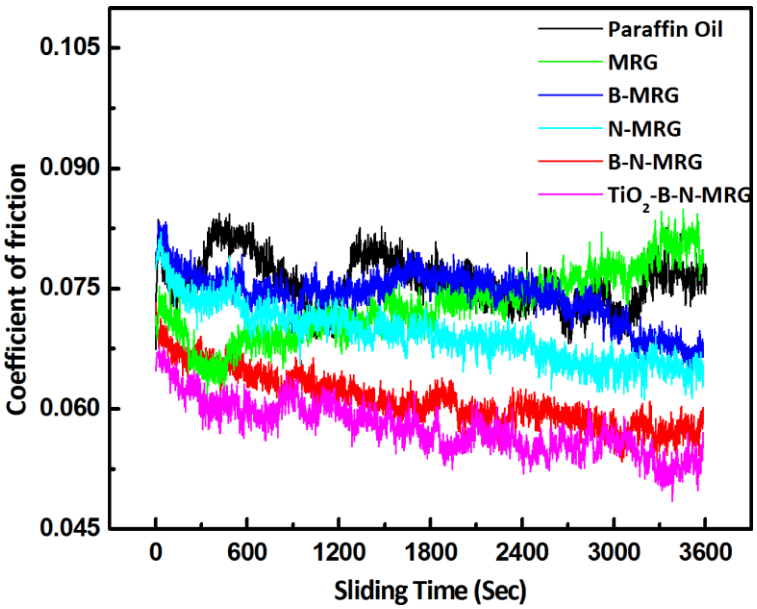

Figure 6.9. Variation in coefficient of friction as a function of time in the presence of MRGs nanomaterials in paraffin oil; Load: 392N, sliding speed: 1200 rpm, temperature: 75 °C, test duration: 60 min., concentration of MRGs: 0.15 % w/v

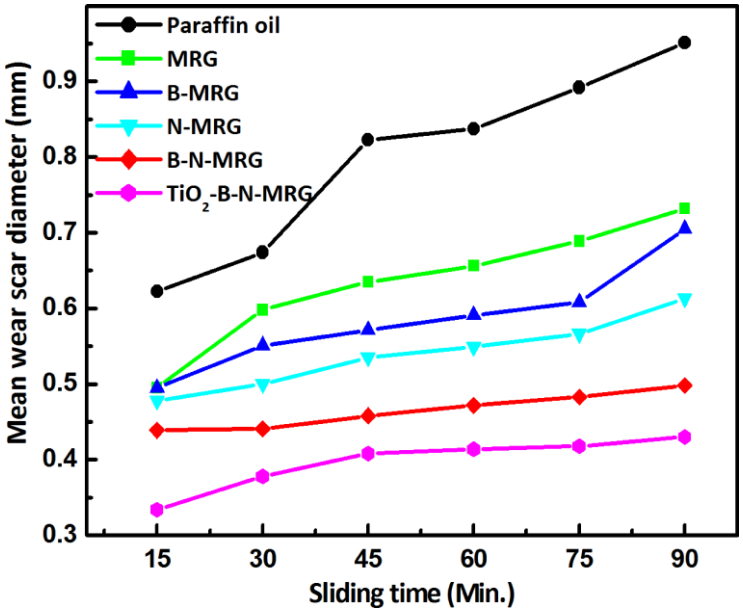

Figure 6.10. Variation of mean wear scar diameter with time for paraffin oil containing 0.15% w/v of different MRGs nanomaterials at 392N applied load

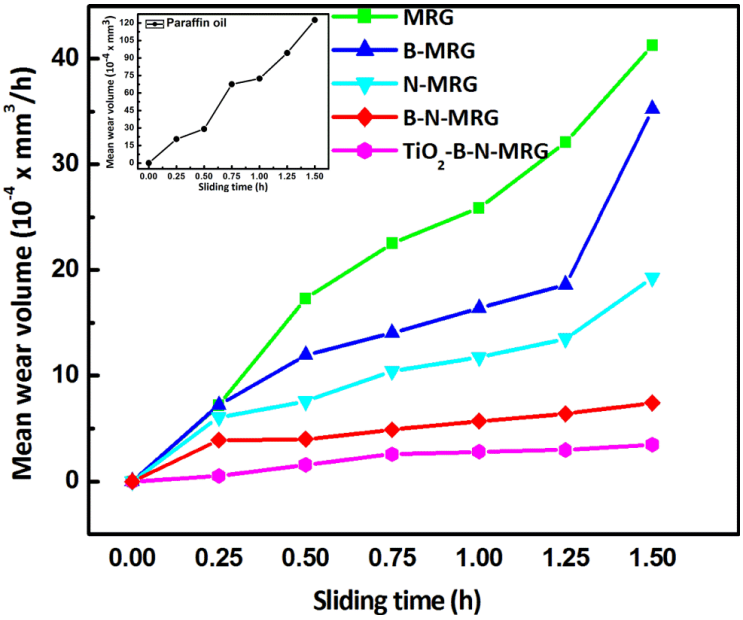

Figure 6.11. Variation of mean wear volume with time for paraffin oil containing 0.15% w/v of different MRGs nanomaterials at 392N applied load

Table 6.1. Wear rates of paraffin oil in absence and presence of MRG based nanomaterials as antiwear additives at 392N applied load for 90 min test duration

Sl. No.	Lubricant additives	Wear rate (10^{-4} x mm^3/h)	
		Running-in	Steady-state
1	Paraffin oil	84.48	53.32
2	MRG	31.09	19.09
3	B-MRG	18.75	09.08
4	N-MRG	13.13	06.14
5	B-N-MRG	05.91	03.02
6	TiO_2-B-N-MRG	03.52	00.79

6.2.3.3. Effect of load

Figure 6.12 shows relationship between the applied load and mean wear scar diameter of different synthesized additives in paraffin oil at 0.15% w/v for 30 min sliding time. The increase of applied load results in the increase in the MWD value. This may be due to the fact that with increase of applied load, the film thickness between the contacting surfaces decreases resulting into the increase in the direct

contact of asperities [Ji *et al*.(2005)]. The values of MWD are found to be much larger in case of surface lubricated with base oil at each tested load than the surface lubricated with additives. Initially at 294N load, the MWD is very large in the absence of additives but in the presence of MRG, B-MRG and N-MRG it is remarkably reduced. The value of MWD is further reduced upon co-doping of boron and nitrogen in MRG and reaches the minimum value for the blend of TiO_2-B-N-MRG. This behavior of different additives follows the same order till 588N except MRG, where a sudden increase in the MWD has been observed. Beyond 588N load the thin film fails to sustain the load in the case of blends of B-MRG and N-MRG in paraffin oil. On further increasing the load up to 686N, admixtures of B-N-MRG and TiO_2-B-N-MRG successfully bear the load, however, the MWD values are found to be much larger in the former case than the latter one. Moreover, as expected the load bearing ability of TiO_2-B-N-MRG is found to be maximum up to 784N.

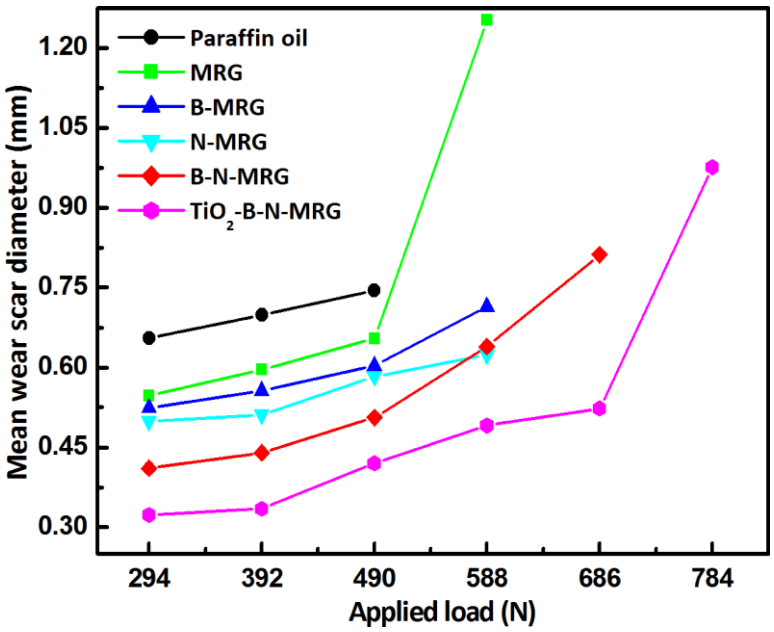

Figure 6.12. Variation of mean wear scar diameter with applied load for paraffin oil containing 0.15% w/v of different MRGs nanomaterials for 30 min test duration

Application of MRG as lubricating oil additive under extreme conditions has been limited due to its poor adherence with sliding surface [Berman *et al*.(2014)]. The load bearing ability of MRG is improved upon doping of individual boron and nitrogen atom which enhanced the adherence property of the MRG. The adherence property of MRG is further improved upon co-doping of B and N atoms which clearly reflects that the nature of tribofilm/s formed for the surface lubricated with B-N-MRG

is entirely different from the film/s generated in case of surface lubricated with B-MRG and N-MRG. The excellent load bearing ability of B-N-MRG may be due to the fact that under lubricating conditions it adsorbed on the sliding surfaces and under extreme conditions B-N-MRG decomposed to form *in situ* protective tribochemical film which is composed of boron nitride as it was obtained in our previous chapter. However, TiO_2 reinforced MRG hybrid nanomaterial further enhanced the load bearing ability of B-N-MRG which is due to the presence of additional TiO_2 nano bearings providing low shear strength between steel-steel interfaces. Therefore, these hybrid nanomaterials exhibit excellent antiwear properties in a relatively wide range of applied load.

6.2.3.4. Coefficient of friction test

The steady-state period is very important for the life-span of all engineering components under tribostress. In order to investigate the behavior of different graphene based hybrid nanomaterials towards steady-state coefficient of friction, the standard test ASTM D5183 has been performed. Prior to perform steady-state COF, initially the test has been conducted under the load of 392N at 600 rpm for 60 min time duration with heating at 75 $^{\circ}$C to ensure the completion of running-in period for all the studied additives. The obtained results are mentioned in Figure 6.13. On comparing Figure 6.8 with Figure 6.13, it is evident that on decreasing the sliding speed (from 1200 to 600 rpm) MWD values decrease whereas COF values somewhat increase in all cases. After this, the steady-state COF test has been performed for all the tested additives by varying the applied loads stepped by 98N at each 10 min of time and their corresponding values are displayed in Figure 6.14. Initially, the value of frictional torque is found to be somewhat higher in absence of additives than the surface lubricated with additives. As the load and time increase, the difference in the frictional torque values between base lube and blends of additives becomes very large. At each load, lower and stable frictional torque values w.r.t. time is observed in presence of additives. Besides this, there is drastic increase in the frictional torque value in case of paraffin oil at 1078N load causing seizure between tribopairs. However, for the tribopairs lubricated with MRG, B-MRG, N-MRG, B-N-MRG and TiO_2-B-N-MRG, the seizure occurred at 1078, 1274, 1274, 1372 and 1470 N load, respectively, which is due to the rupture of tribofilm resulting break in steady-state. These results further prove the friction-reducing and antiwear properties of hybrid graphene based nanomaterials under the extreme conditions. The findings of this test also strengthen the objective of the present communication that the sustainability of MRG towards higher load conditions should be enhanced. That is witnessed by the

observed synergistic interaction of B-N-co-doped-MRG at steel-steel interface and further enhancement in tribological properties due to TiO_2 nano bearings in TiO_2 reinforced B-N-co-doped-MRG.

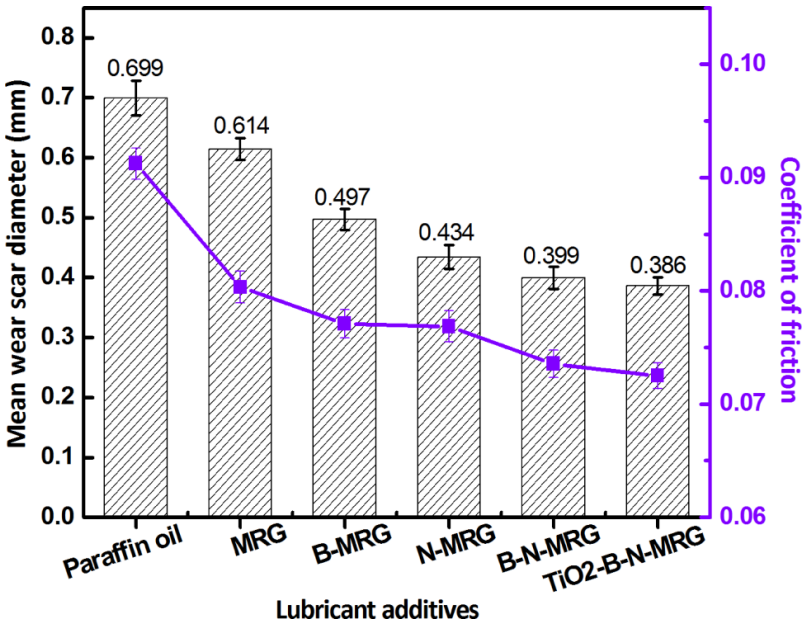

Figure 6.13. Variation in mean wear scar diameter and coefficient of friction in the presence of MRGs nanomaterials in paraffin oil. Load: 392N, sliding speed: 600 rpm, temperature: 75 °C, test duration: 60 min., concentration of MRGs: 0.15 % w/v

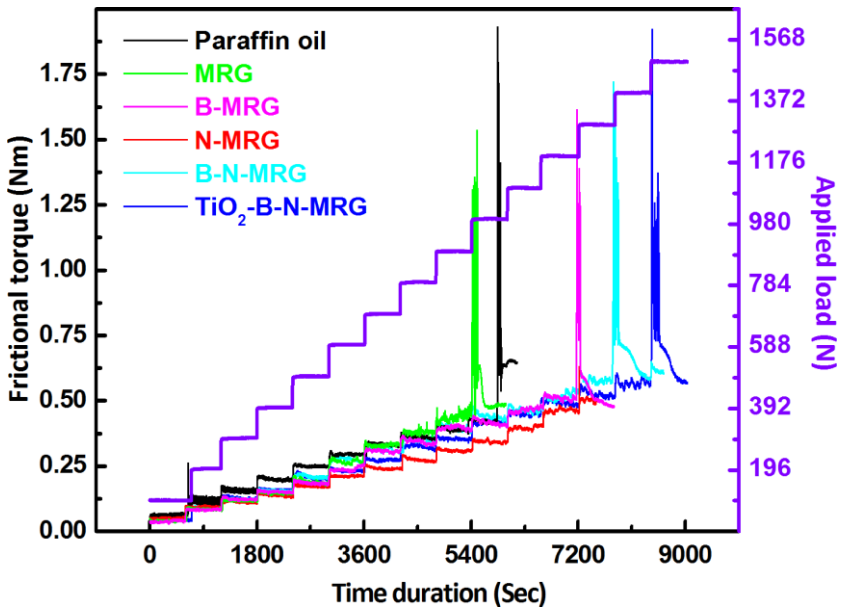

Figure 6.14. Variation of frictional torque as a function of step loading and time for different graphene based nanomaterials. sliding speed: 600 rpm, temperature: 75 °C, concentration of MRGs: 0.15 % w/v

6.2.3.5. Surface Characterization

The surface morphology of wear scar formed on sliding surfaces has been studied by scanning electron microscopy (SEM) and contact mode atomic force microscopy (AFM) techniques. Figure 6.15 shows SEM images of worn steel surfaces lubricated with base oil and blends (0.15 % w/v) of each additive under the load of 392N for 60 min test duration. The worn area in presence of base oil exhibited very large MWD (0.733mm) with huge surface destruction attributed to the plastic deformation on the steel surface under the test conditions. However, in presence of the additives, remarkable smoothening of surfaces has been observed which is in conformity with the order of antiwear properties of different additives. From the SEM images (inset), it can be clearly seen that the value of MWD is successively reduced upon doping of B/N, co-doped-B-N and finally TiO_2-reinforced co-doped-B-N to MRG which correlates well with their observed tribological behavior. There are some pad-like structures visible on the surface of wear track lubricated with additives which are supposed to be due to adsorbed graphene sheets under the tribostress. In order to prove the suitability of these hybrid graphene based nanomaterials at higher load, the SEM-images of the wear track were also taken at higher load i.e., 588N for 30 min of test duration. Figure 6.16 shows the SEM-images of surface added with blends of MRG, B-MRG, B-N-MRG and TiO_2-B-N-MRG. These images also exhibit the effect of dopant and/or reinforcement of TiO_2 to MRG by reducing corresponding MWD values to a greater extent.

The surface topography of worn steel surfaces in presence and absence of graphene based materials in base oil has been compared using contact mode AFM. The *2D* and *3D* AFM-images along with surface roughness values (line roughness; Rq and area roughness; Sq) of steel surfaces under the load of 392N for 60 min. time duration are displayed in Figure 6.17. The line roughness of each of the worn surfaces has been taken across the sliding direction. The values of surface roughness are found to be much higher in absence of additives (Sq= 674 nm; Rq= 670 nm) whereas in presence of MRGs these values are surprisingly reduced (Sq= 105-40 nm; Rq= 149-39 nm). Among the studied MRGs, both B-N-MRG and TiO_2-B-N-MRG show the maximum reduction in surface roughnessess up to~94%. The AFM-images lubricated with these additives clearly show some pad-like deposition along with sliding

direction. The pad like deposition on the sliding track is a consequence of adsorbed nanomaterials and/or synergistic effect of co-doped B-N-MRG forming *in situ* tribochemical film on the steel-steel interface. The AFM-observation also strengthens the SEM results under the similar test conditions. The AFM-images of studied graphene based additives are also taken at 588N load for 30 min test duration, Figure 6.18. These AFM-images show the similar trend towards the surface smoothening as observed in the above case. Thus, these nanomaterials have potential to be used under high load conditions, too.

6.2.3.6. Tribochemistry

In order to explore the chemical composition of tribofilm, the XPS spectra of the steel surface lubricated with TiO_2-B-N-MRG under ASTM D5183 has been recorded. Each spectrum has been deconvoluted with XPS Peak software after subtracting the Shirley background. Figure 6.19 shows the curve fitted XPS-spectra of C 1s, B, 1s, N 1s, O1s, Ti 2p and Fe 2p of the lubricated steel surface. Figure 6.19(a) shows that the core level spectra of C1s have been deconvoluted into three similar peaks as observed in case of TiO_2-B-N-MRG with binding energies of 284.8, 286.3 and 287.9 eV corresponding to sp^2C–sp^2C, N-sp^3C and C=O moieties respectively [Han *et al*.(2013)]. Besides this, on combining the binding energies of B 1s (Figure 6.19 (b)) with N 1s signal (Figure 6.19 (c)) appearing at 189.8 eV and 398.6 eV, respectively confirmed the formation of boron nitride between tribopairs [Shulga *et al*.(1990), Hendrickson *et al*.(1969)]. However, there is no significant shift in the binding energies of Ti $2p_{1/2}$ and Ti $2p_{3/2}$ signals showing that TiO_2 nanoparticles are tribosintered on the metallic surface (Figure 6.19 (d)) [Reddy *et al*.(2010)]. The iron of the steel surface was oxidized to Fe_2O_3 under lubricating conditions which is evident from the observed signals 711.8 eV for Fe 2p and 530.6 eV for O 1s spectra (Figures 6.19 (e) and (f)) [Li *et al*.(2010)]. Therefore, it can be reasonably concluded that the TiO_2-B-N-MRG nanomaterial has proven its excellent tribological behavior by virtue of forming *in situ* protective boron nitride tribofilm and graphene layers deposited on the steel-steel interfaces under tribostress conditions. The reinforced TiO_2 nanoparticles act as nano bearings to form uniform layer which prevents direct meal-metal contact and thus reducing friction and wear.

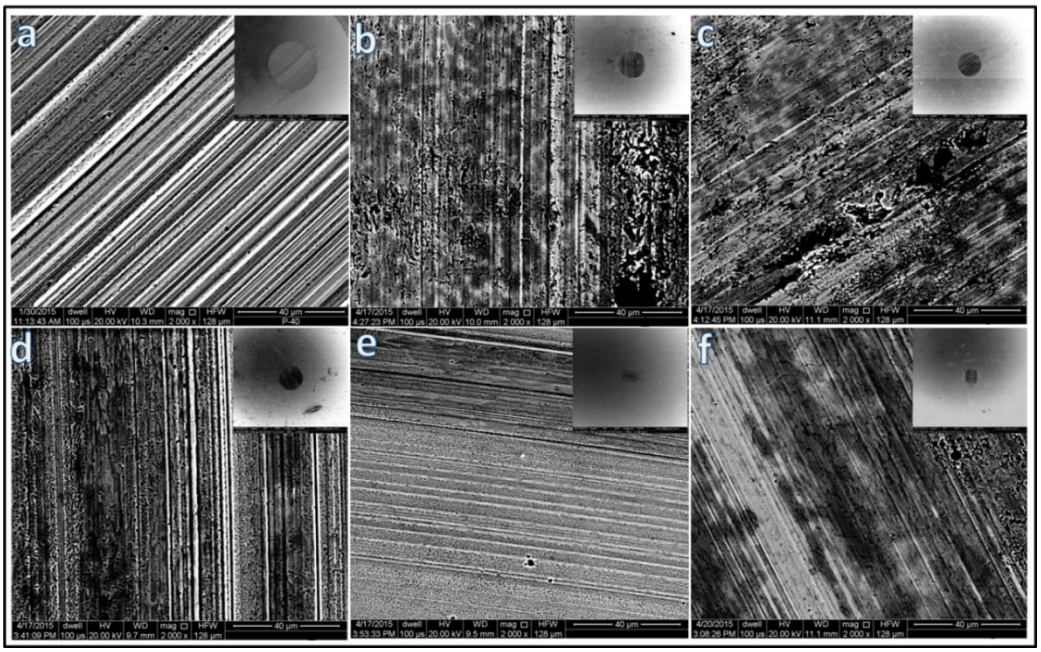

Figure 6.15. SEM micrographs at different magnifications of the worn steel surface lubricated with different additives (0.15% w/v) in paraffin oil for 60 min test duration at 392N applied load: (a) Paraffin oil, (b) MRG, (c) B-MRG, (d) N-MRG, (e) B-N-MRG and (f) TiO_2-B-N-MRG

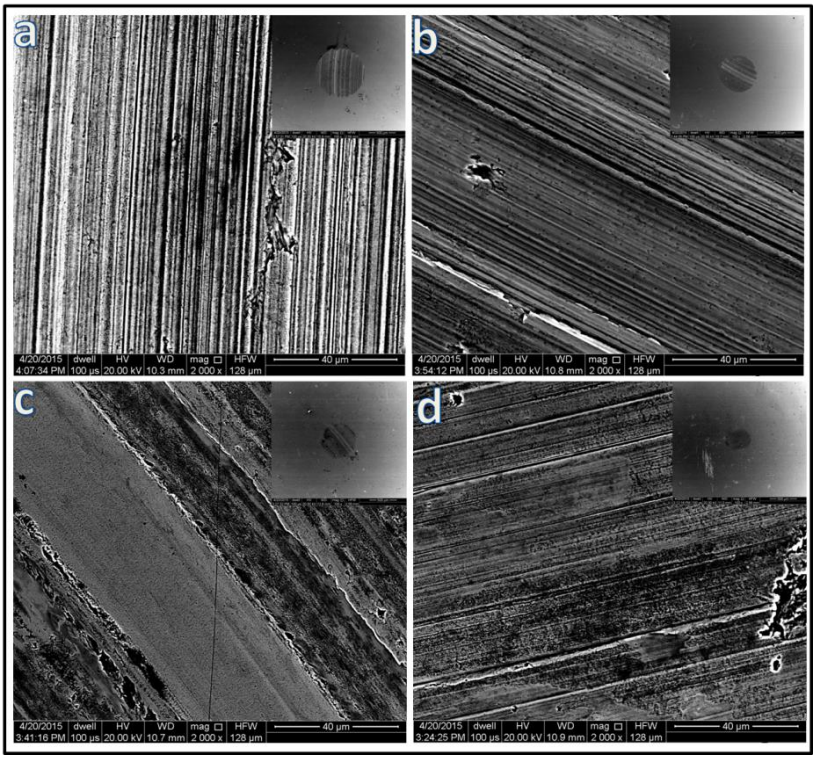

Figure 6.16. SEM micrographs at different magnifications of the worn steel surface lubricated with different additives (0.15% w/v) in paraffin oil for 30 min test duration at 588N applied load: (a) MRG, (b) B-MRG, (c) B-N-MRG and (d) TiO_2-B-N-MRG

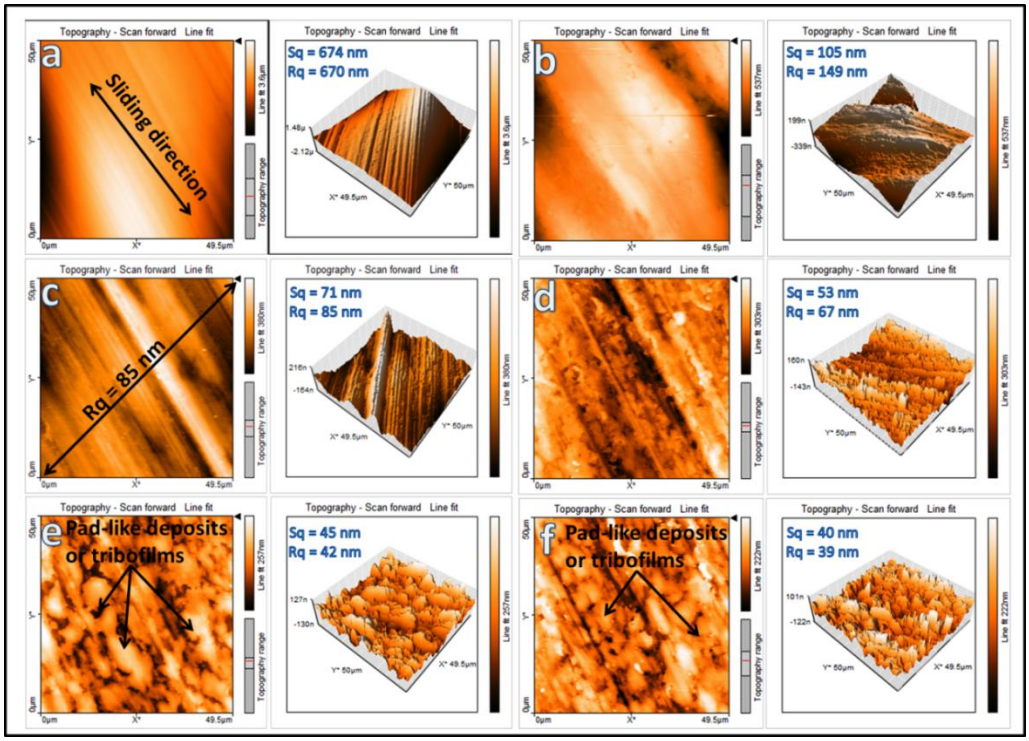

Figure 6.17. 2*D* and 3*D*-AFM images of the worn steel surface lubricated with different additives (0.15% w/v) in paraffin oil for 60 min test duration at 392N applied load: (a) Paraffin oil, (b) MRG, (c) B-MRG, (d) N-MRG, (e) B-N-MRG and (f) TiO_2-B-N-MRG

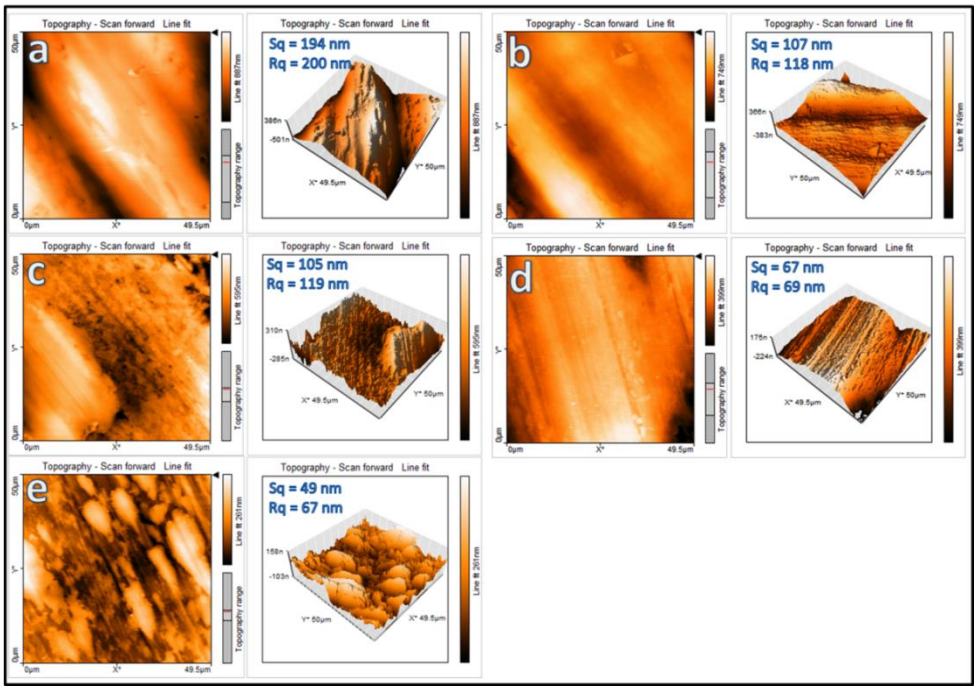

Figure 6.18. 2*D* and 3*D*-AFM images of the worn steel surface lubricated with different additives (0.15% w/v) in paraffin oil for 30 min test duration at 588N applied load: (a) MRG, (b) B-MRG, (c) N-MRG, (d) B-N-MRG and (e) TiO_2-B-N-MRG

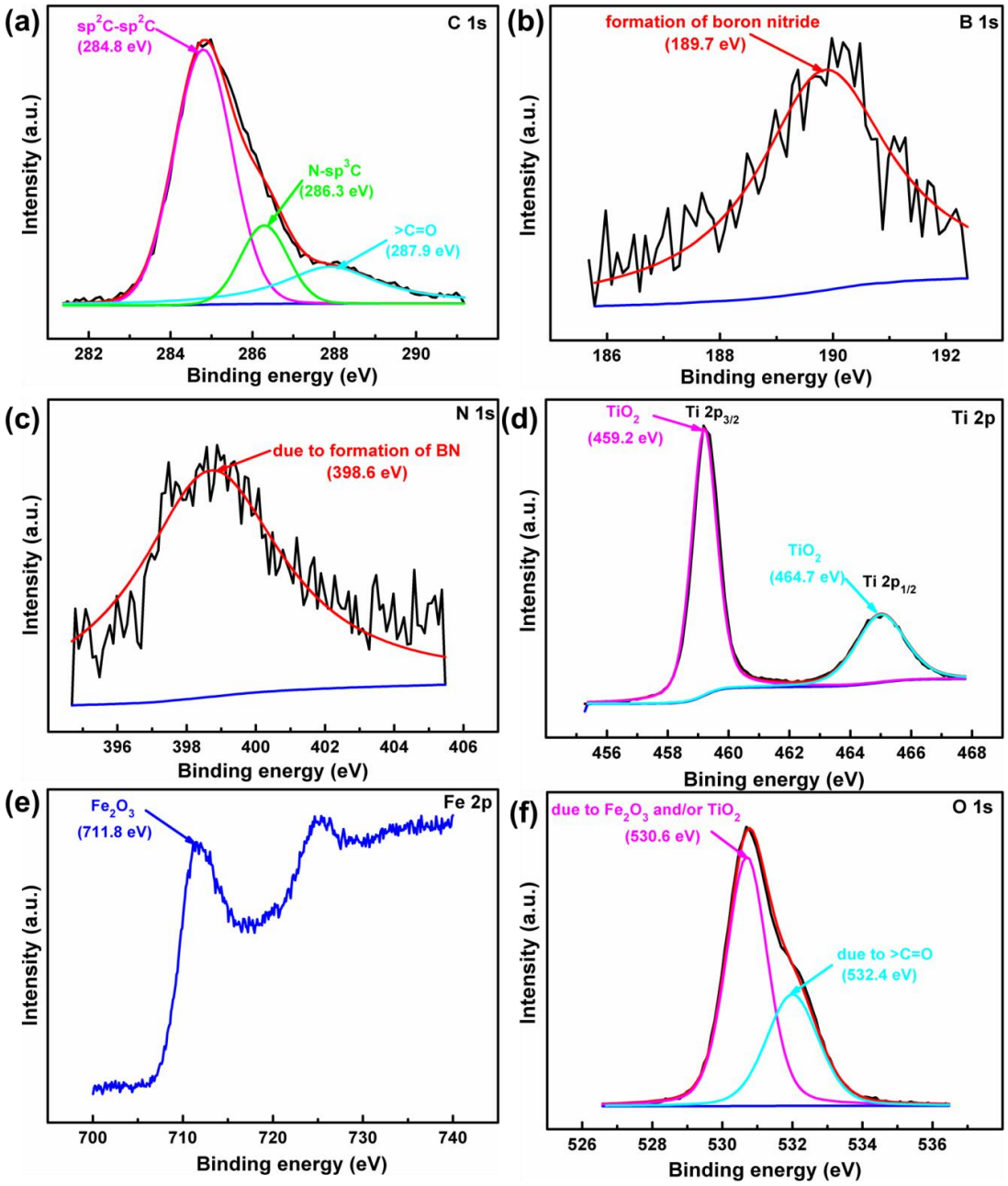

Figure 6.19. Deconvoluted XPS spectra of the tribofilm formed on the steel surface lubricated with TiO_2-B-N-MRG nanomaterial under ASTM D5183 test standard: (a) C1s spectra, (b) B1s spectra, (c) N1s spectra, (d) Ti2p spectra, (e) Fe 2p spectra and (f) O1s spectra

6.2.3.7. Proposed mechanism

Based on the observed tribological and surface characterization results, the excellent tribological properties of the studied MRGs nanomaterials acting as novel additives in paraffin have been proved. Among studied MRGs, both B-N-MRG and

TiO_2-B-N-MRG nanomaterials exhibit much improved tribological properties. The enhanced tribological properties of B-N-co-doped-MRG and TiO_2-reinforced-B-N-co-doped-MRG are due to the following reasons-

Initially, these nanomaterials get uniformly adhered in between the tribopairs. Under high stress conditions, the anchoring behavior of graphene is poor in comparison to doped and reinforced graphene based nanomaterials.[345] Under extreme conditions (high load and high temperature), these doped elements boron and nitrogen reacted themselves to form *in situ* protective tribofilm to minimize asperity-asperity adhesion which is evident from its much smaller MWD value in case of B-N-co-doped-MRG. The formation of protective tribofilm is time-dependent and it is facilitated as the time increases [Cavdar *et al*.(1991)]. Furthermore, in case of TiO_2-B-N-MRG, the TiO_2 nanoparticles deposited in between MRG surfaces prevent agglomeration. Being spherical in shape, TiO_2 nanoparticles act as nano bearings in between the both MRG layers and tribopairs, therefore, facilitate the sliding phenomenon of MRG layers under high stress conditions reducing friction and wear. Thus, excellent tribological properties of B-N-codoped-MRG may be due to the formation of *in situ* BN tribofilm under tribostress condition on the sliding surfaces. These properties are further enhanced in case of TiO_2-reinforced-B-N-MRG nanomaterial (Figure 6.19) due to TiO_2 nano bearings and/or tribosinterization.

6.3. Conclusions

The microwave synthesis of few layered thick reduced graphene oxide (MRG), B-MRG, N-MRG, B, N-co-doped-reduced graphene oxide (B-N-MRG) and TiO_2-reinforced-B-N-MRG (TiO_2-B-N-MRG) nanomaterials have been successfully synthesized and characterized by various states of the art techniques like Raman, powder XRD, SEM with EDX, HRTEM and XPS. As novel lubricant additives, the as-prepared B-N-MRG and TiO_2-B-N-MRG nanomaterials possess appreciable dispersion stability in paraffin oil. Friction and wear characteristics of these nanomaterials were evaluated using four-ball lubricant tester at optimized concentration (0.15% w/v). The observed tribological results show that B/N/B-N doped MRG and TiO_2-reinforced MRG exhibit tremendous reduction in MWD (from 0.733 to 0.366 mm) and COF (from 0.0756 to 0.0564) values but load carrying ability

gets significantly enhanced from 1078 to 1470N. In addition to this, studied additives exceptionally reduced the steady-state wear rate in the range of 64-98%. SEM and AFM studies revealed that there is some pad-like deposition on the sliding surfaces lubricated with B-N-MRG and TiO_2-B-N-MRG which may be the consequence of *in situ* formed tribofilm preventing metal-metal contact. The XPS analysis of tribofilm formed on the surface lubricated with TiO_2-B-N-MRG confirmed the presence of graphitic carbon, boron nitride and tribosintered TiO_2 nanoparticles. Above results suggest that the synthesized B-N-MRG and TiO_2-B-N-MRG nanomaterials are the potential candidates to be developed as SAPS-free antiwear lubricant additives under boundary lubricating conditions. Despite its low thickness, MRGs have improved anti-frictional properties and imparted relatively high wear resistance that makes them attractive materials for various applications in tribology.